Available online at www.sciencedirect.com
SCIENCE DIRECT®
International Journal of Multiphase Flow 30 (2004) 1451–1484
International Journal of Multiphase Flow
www.elsevier.com/locate/ijmulflow

Experimental investigation and theoretical modeling of liquid entrainment in a horizontal tee with a vertical-up branch

K.B. Welter [a,*], Q. Wu [b], Y. You [b], K. Abel [b], D. McCreary [b], S.M. Bajorek [a], J.N. Reyes Jr [b]

[a] *Office of Nuclear Regulatory Research, US Nuclear Regulatory Commission, U.S.A*
[b] *Department of Nuclear Engineering, Oregon State University, U.S.A*

Received 4 November 2003; received in revised form 11 August 2004

Abstract

This article describes a comprehensive literature review of liquid entrainment in horizontal pipes with vertical-up branches. Deficiencies in the available data and correlations were identified. The Air–water Test Loop for Advanced Thermal–hydraulic Studies (ATLATS) was constructed and entrainment onset and steady-state data were collected for a wide range of flow conditions. Using new insights gained from experimental testing, the authors developed a model for predicting the onset of entrainment and steady-state entrainment rate. Previously published correlations, along with the new model, are compared against all available data. The new model shows very good agreement with the onset data, but is not very good at predicting branch quality at high liquid flow rates.

Keywords: Phase separation; Liquid entrainment; Tees; LOCA; Advanced reactor

1. Introduction

The study by Rouse (1956) on the development of noncirculatory waterspouts was one of the first experiments to explore the fundamentals of liquid entrainment. Rouse focused on

* Corresponding author. Tel.: +1 301 415 5740; fax: +1 301 415 5160.
E-mail address: kbw@nrc.gov (K.B. Welter).

0301-9322/$ - see front matter © 2004 Elsevier Ltd. All rights reserved.
doi:10.1016/j.ijmultiphaseflow.2004.08.001

noncirculatory water spouts that form in the low-pressure zone produced by radial flow toward an intake in either of the two fluid layers with different densities. In one experiment, Rouse used a tank open to the atmosphere filled with water and placed a pipe just above the water surface. A vacuum was then created in the pipe causing the surrounding air to rush into the pipe. As the vacuum was increased, the resulting increase in air velocity caused a noncirculatory waterspout to form on the liquid surface as shown in Fig. 1.1. The purpose of Rouse's study was to determine the rate of air flow necessary to develop a waterspout just to the point where water began to enter the vertical pipe.

In the following decades, researchers, motivated by applications in the petroleum, water processing, and nuclear industries, to name a few, expanded on Rouse's initial study. Researchers began to study more complicated geometries and run experiments with a wider range of flow conditions. The geometries ranged from horizontal pipes with vertical-up or -down and side branches to vertical-up or -down pipes with side branches. Both tee- and wye-shaped junctions were studied. In these more complex experiments, the phenomenon no longer resembled the simple noncirculatory water spout observed by Rouse. Hence the coinage of the terms "phase separation" and "liquid entrainment" to better describe the process by which two concurrently flowing liquids of different densities can separate when they flow past a break or a branching pipe. More recently, the phase separation phenomena unique to a horizontal pipe with a vertical-up branch geometry has become particularly important in the accident analysis of new or advanced pressurized water nuclear reactors, which is the focus of this study.

Under certain critical conditions when liquid and gas concurrently enter a horizontal tee with an upward-oriented vertical branch, liquid can be entrained through the branch as shown in Fig. 1.2. The study of liquid entrainment or phase separation in tees of this geometry has traditionally been divided into two steps: onset of liquid entrainment and steady-state entrainment rate. For this study, consider an empty pipe like that shown in Fig. 1.2 with a constant gas flowing from the inlet and out the branch and outlet. Slowly start to fill the pipe with liquid. As the liquid level rises in the mainline, instabilities can form on the liquid surface and if the liquid level and gas flow rate are high enough, water can begin to entrain out the vertical branch. This critical point is called the onset of entrainment and the associated parameter used to describe it is the onset of liquid entrainment gas chamber height, h_b. The quality in the branch is just slightly under one at this time. With the same gas flow rate, continue to fill the mainline past the onset of entrain-

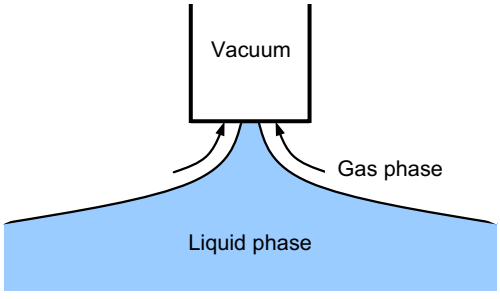

Fig. 1.1. Surface profile of waterspout in air (Rouse, 1956).

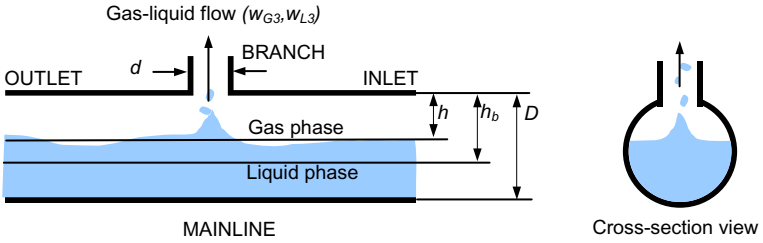

Fig. 1.2. Surface profile of phase separation in a horizontal pipe with an upward-oriented vertical branch.

ment. Liquid will entrain at a higher rate as the liquid level rises and the quality in the branch will drop dramatically. Stop increasing the liquid and maintain a constant liquid and gas flow, and a steady-state gas chamber height can be obtained, h. By using the onset of liquid entrainment gas chamber height (which is a function of gas flow rate), h_b, and the steady-state gas chamber height, h, the quality in the branch can be predicted with an appropriate correlation. Accurately predicting the branch quality based on these parameters is the central issue of liquid entrainment studies. Specifically, in a new pressurized water reactor, this tee geometry is part of a safety-related component, and accurate prediction of branch quality is very important. Before going into the details of nuclear reactor thermal–hydraulics, a basic overview of the primary system of a new pressurized reactor may be helpful.

The main cooling mechanism in new pressurized water reactors is water at high temperature and pressure. Under normal conditions, shown in Fig. 1.3, the plant is completely full of water which is heated by the nuclear fuel in the reactor core. Hot water exits the hot leg, travels through the tubeside of the steam generator, is cooled by feedwater, and is pumped back to the reactor

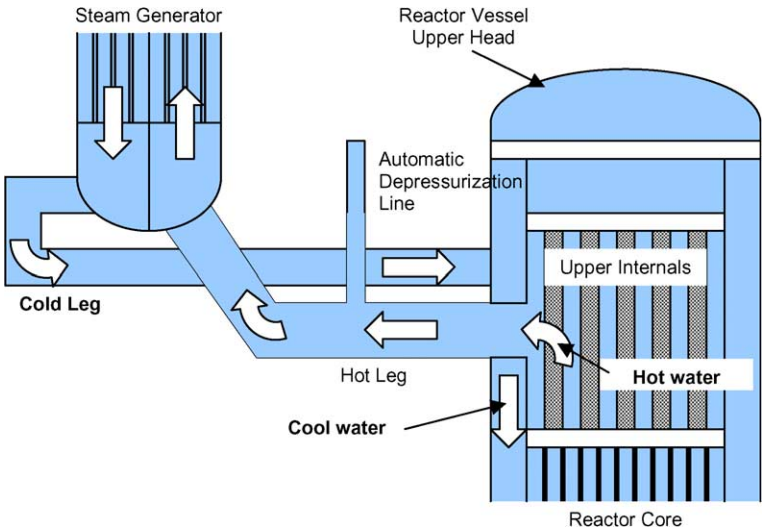

Fig. 1.3. Normal operating conditions. Primary side of a new pressurized water reactor.

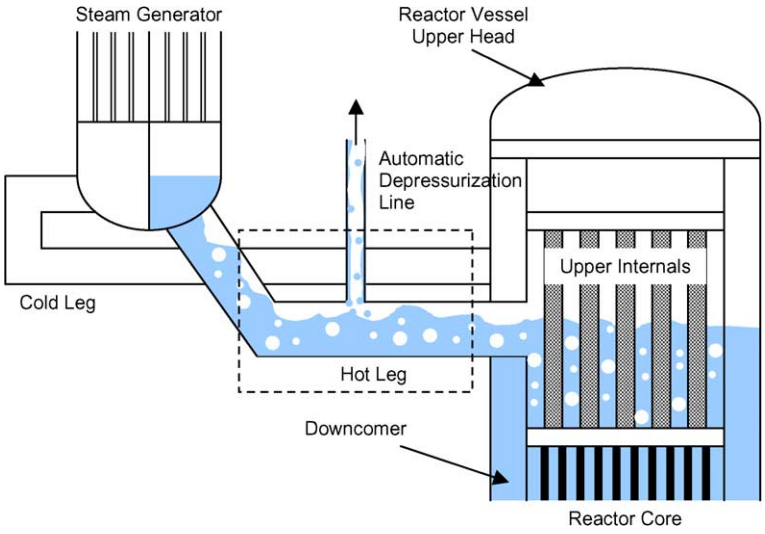

Fig. 1.4. Loss-of-coolant accident. Primary side of a new pressurized water reactor.

core via the cold leg, thus completing the primary heat transfer cycle. Under accident conditions, such as a loss-of-coolant accident, the plant can depressurize rapidly, causing a large part of the cooling water to flash to steam. This creates a two-phase mixture in the primary piping system as shown in Fig. 1.4.

Of special interest during a loss-of-coolant accident is the liquid entrainment which can take place as water and steam encounter a vertical automatic depressurization line off the hot leg (see dashed box in Fig. 1.4). If the decay heat produced from reactor is high enough, it can boil off large amounts of primary coolant. The resulting steam from the reactor vessel flows through the path of least resistance, which is typically out the automatic depressurization lines. If the flow reaches a critical velocity, water from the partially filled hot leg can be entrained out the depressurization line, removing coolant from the primary system. Maintaining core cooling is of the utmost importance. Therefore, loss-of-coolant accident analyses must make every attempt to accurately quantify the amount of primary coolant removed due to this phenomenon.

The lack of thorough understanding of phase separation phenomena has been frequently mentioned. In 1997, phase separation in tees was identified as a "high-ranked" phenomenon in the AP600 Small Break Loss-of-Coolant Accident (SBLOCA) Phenomena Identification and Ranking Technique (PIRT). The OECD/CSNI workshop on "Transient Thermal-Hydraulic and Neutronics Codes Requirements" (November 5–8, 1996) also identified the need for improved phase separation models in system analyses codes.

The first task of this research project was to conduct a comprehensive literature review to identify current data and correlation inadequacies with respect to horizontal tees with a vertical-up branch. Several deficiencies were discovered and an experimental facility was constructed to extend the currently available database. Data was collected that is more representative of conditions that would be experienced in a new pressurized water reactor. This article proposes a new model for predicting liquid entrainment.

2. Literature review

Table 2.1 presents a chronological list of previous investigations relevant to liquid entrainment at tee junctions with an upward-oriented vertical branch. From the literature review it is evident that the previous experimental investigations have the following common deficiencies with respect to analyzing new reactor accident scenarios.

2.1. Tee branch scaling

Most of the test data were obtained in experimental facilities whose geometric conditions were too far from the prototypic cases. For instance, a plot of d/D versus D shown in Fig. 2.1 summarizes the test conditions for entrainment investigations. All the test data that supported the existing correlations were obtained in the left portion of the plot, whereas the system conditions of new pressurized water reactors are generally at the far right side. Test data with greater d/D ratio and larger D size would be of great value for the evaluation of the correlations scalability.

Table 2.1
Chronological summary of liquid entrainment studies

Date	Author(s)	Institute	Experiments	
			Flow regime(s)[a]	D/d[b]
1981	Crowley et al.	Creare Inc.	S, SL	12
1984	Reimann et al.	KfK	S	34, 26, 17, 10
1986	Schrock et al.	UCB	S	31, 25, 17, 10
1989	Maciaszek et al.	CEA	S	7
1991	Yonomoto	JAERI	S	19, 17, 9

[a] S = Stratified or stratified-wavy and SL = Slug.
[b] Mainline-to-branch diameter ratio.

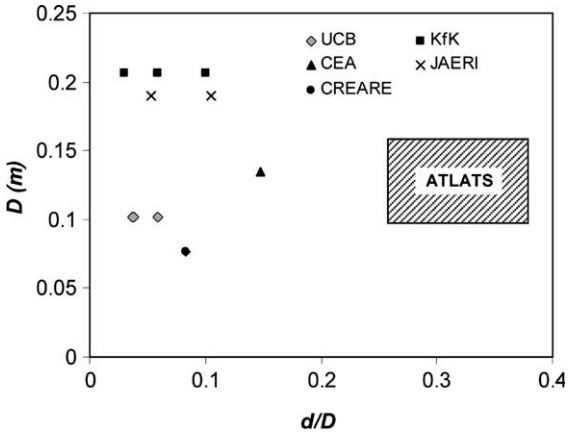

Fig. 2.1. Comparison of prototypic geometry to previous experimental facilities (D: hot leg diameter; d: branch diameter).

2.2. Inlet conditions

Almost all the reported test facilities had a gas-liquid mixer at the inlet of the horizontal duct, which differs from the prototypic hot leg inlet configuration shown in Fig. 1.4. For instance, the automatic depressurization branch in the new reactor designs is close to the hot leg inlet. Hence, the flow development length as well as the inlet condition should be examined for the correlation evaluation. Specifically, the transition between stratified flow to slug flow may be altered due to the short inlet length and the disturbances on the mixture surface at the hot leg inlet.

2.3. Hot leg flow regimes

Most of the steady-state entrainment rate data were collected in the fully developed stratified flow regime as shown in Table 2.1. An analysis to determine the most commonly encountered flow regimes during plant blowdown is contained in the Scaling section of this article. The compact nature of the reactor primary side could greatly influence how much the flow can develop, which means that under accident conditions, the flow in the hot leg is most likely not only stratified.

2.4. Onset of entrainment correlations

Large discrepancies exist among different entrainment onset correlations as demonstrated in Fig. 2.2 and summarized in Table 2.2 in the form of the dimensionless critical gas space height (h_b/d) versus the gas phase Froude number based on the branch inlet gas flow velocity and the branch diameter. The correlations of Schrock et al. at Berkeley (Lawrence Berkeley of the University of California, Berkeley) and of Smoglie at KfK (Kernforshungszentrum Karlsruhe GmbH, Karlsreuhe, Germany), which were developed for relatively small branch sizes ($D/d > 17$), are very close to each other. For larger break sizes, however, the correlation of Maciaszek and Micaelli

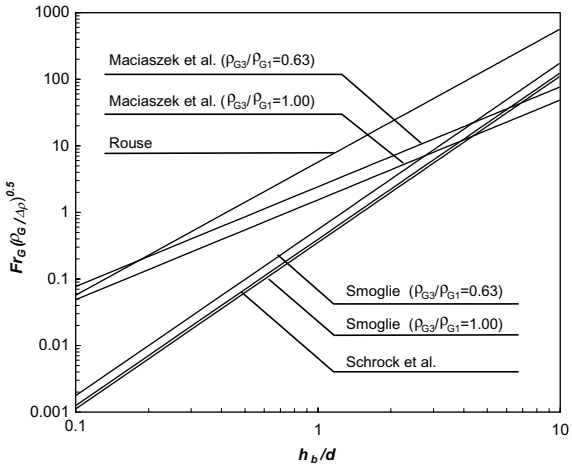

Fig. 2.2. Entrainment onset correlations.

Table 2.2
Entrainment onset correlations

Reference	Onset correlation
Smoglie (1984)	$h_b = 1.67\left(\frac{w_{G3}^2}{\rho_G \Delta\rho g \pi^2}\right)^{1/5}$
Schrock et al. (1986)	$Fr_G\left(\frac{\rho_G}{\Delta\rho}\right)^{1/2} = \left(\frac{V_{G3}}{\sqrt{gd}}\right)\left(\frac{\rho_G}{\Delta\rho}\right)^{1/2} = 0.395\left(\frac{h_b}{d}\right)^{2.5}$
Maciaszek and Micaelli (1986)	$h_b = 0.88\left(\frac{w_{G3}^2}{\rho_G \Delta\rho g d^2}\right)^{1/3}$

(1986) at CEA (Centre d'Étude Nucléaire de Grenoble, France) differs substantially from the others, indicating that the break size has a significant effect on the entrainment onset conditions.

2.5. Entrainment rate correlations

In Fig. 2.3, discrepancies were also observed for different entrainment rate correlations summarized in Table 2.3. Schrock et al. and Smoglie suggested that the branch gas flow quality could be correlated by h/h_b. These correlations predicted the respective test data reasonable well (Schrock et al.: $x_3 = 0$–0.95; Smoglie: $x_3 > 0.95$), though the two correlations did not agree with each other. The correlation of Yonomoto and Tasaka (1988, 1991) at JAERI (Japan Atomic Energy Research Institute) can also be converted to a function of h/h_b, if the adjustable parameter C is constant. For comparison, we chose the two limits of C that cover the data range presented in the article of Yonomoto and Tasaka (1988, 1991), which are 1.00 and 1.85. The results (Fig. 2.3) show a very different trend from the correlations of Schrock et al. and Smoglie. The entrainment rate model of Maciaszek and Micaelli (1986) is for the case of $h_{lim} > h$, valid only for large branch sizes, where the gas space height for onset of entrainment h_b is close to the slug transition level, h_{lim}. This correlation seems to be close to the predictions of Yonomoto and Tasaka (1988, 1991), but use a very different approach. Nevertheless, all four correlations are associated with h/h_b either directly or indirectly, in spite of the substantial discrepancies among them.

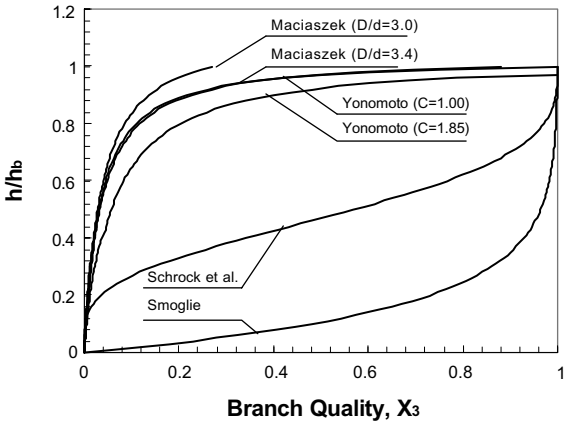

Fig. 2.3. Entrainment rate correlations.

Table 2.3
Entrainment rate correlations

Reference	Entrainment rate correlation
Maciaszek and Micaelli (1986)	$x_3 = 0.98\left(\frac{\alpha}{\alpha+\sqrt{\rho_L/\rho_G}(1-\alpha)}\right)$ $\alpha = h/h_{lim} = 0.441\left(\frac{D}{d}\right)^{2/3}\left(\frac{h}{h_b}\right)$
Schrock et al. (1986)	$x_3 = \left(\frac{h}{h_b}\right)^{3.25}\left(1-\frac{h}{h_b}\right)^2$
Smoglie (1984)	$x_3 = 1-\left(\frac{1.15}{1+\sqrt{\rho_L/\rho_G}}\right)^{2\frac{h}{h_b}}\left[1-0.5\left(\frac{h}{h_b}\right)\left(1+\frac{h}{h_b}\right)\left(\frac{1.15}{1+\sqrt{\rho_L/\rho_G}}\right)^{1-\frac{h}{h_b}}\right]^{0.5}$
Yonomoto and Tasaka (1988)	$x_3 = \frac{\alpha C}{\alpha+\sqrt{\rho_L/\rho_G}(1-\alpha)}$, $\alpha = K_1\left(\frac{h}{h_b}\right)^{5/4}+K_2$ $C = 1.0$ for $\rho_G = \rho_{G3}$ or 1.85 for $\rho_G = \rho_{G1}$ $K_1 = 1.15$, $K_2 = 0$ for $0 < h/h_b < 0.4$ $K_1 = 0.9$, $K_2 = 1$ for $0.4 < h/h_b < 1.0$

3. Scaling analysis

The scaling criteria and the characteristics of the typical phase separation process during a blowdown transient in a new reactor are presented. The target prototypic system is a Westinghouse Electric Inc. AP600 pressurized water reactor. However, the design specifics have been left out due to their proprietary nature.

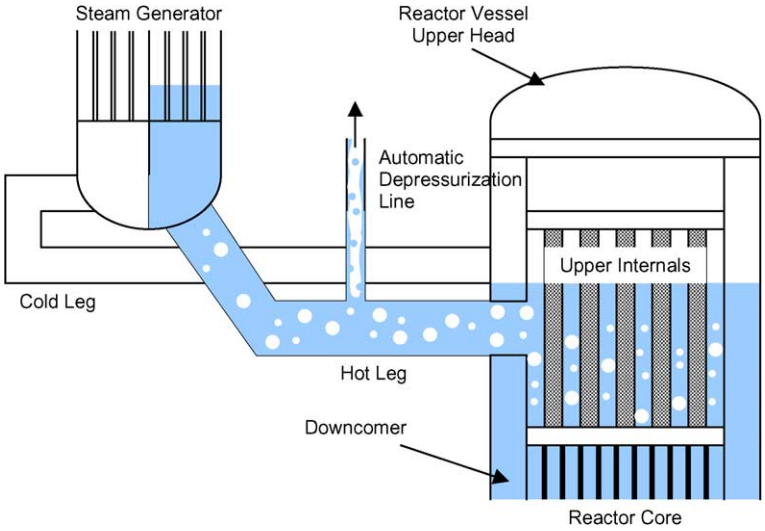

Fig. 3.1. Loss-of-coolant accident sequence or plant blowdown. Submerged hot leg inlet.

3.1. Prototypic phase separation process at vertical tee junction

The initial effort focuses on the phase separation phenomena in a horizontal mainline with a vertical tee branch, similar to a prototypic reactor hot leg with a vertical break or an automatic depressurization line. As demonstrated in Fig. 3.1, a vertical-up branch on a reactor hot leg provides the characteristics of the following processes.

3.1.1. Submerged hot leg inlet, Fig. 3.1

If the reactor vessel mixture level is above the bottom of the hot leg inlet during depressurization, a large amount of liquid is driven out through the vertical-up depressurization line, and the vapor quality in the branch differs from that in the hot leg due to a phase separation process at the tee junction. The flow regime in the hot leg would be most likely bubbly or dispersed bubbly flow. Also, because vapor bubbles tend to rise in the vessel center region, the void fraction at the hot leg opening might be lower than the average value of the mixture. In other words, phase separation phenomena may also occur at the hot leg inlet.

3.1.2. Partially submerged hot leg inlet, Fig. 3.2

Following the initial blowdown, the liquid carryover rate quickly decreases because of the partial uncovering of the hot leg inlet. In this stage, liquid entrainment mechanisms presumably dominate the liquid carryover rate. Depending on the vapor boiloff rate, the flow regime in the hot leg can be stratified or intermittent flow. It is speculated that the short distance to the tee branch form the hot leg inlet would affect the flow regime development. Due to the disturbed surface level in the vessel, liquid slugs may form at the hot leg inlet even for the

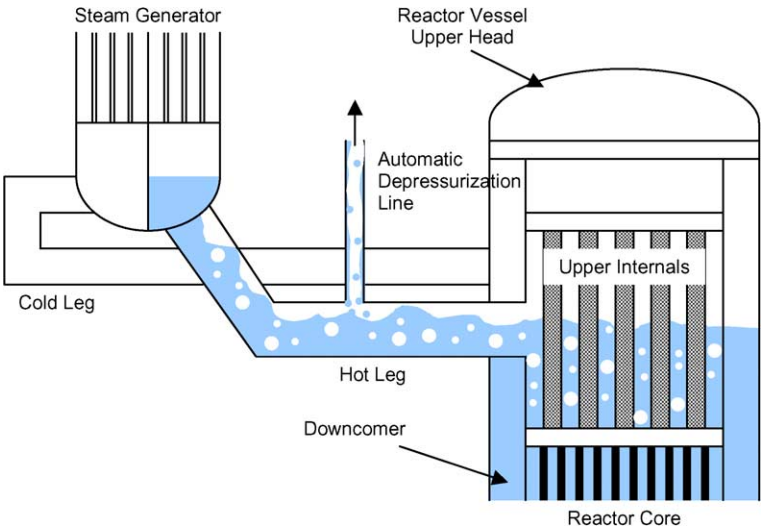

Fig. 3.2. Loss-of-coolant accident sequence or plant blowdown. Partially submerged inlet.

flow that would be categorized as stratified according to the conventional flow regime map Fig. 3.2.

3.1.3. Final steady-state, Fig. 3.3

Eventually, the discharge reaches two possible steady states. If the liquid injection rate is smaller than the boiloff rate, the flow through the branch becomes steady steam flow. Depending on the steam flow rate, the hot leg is either dry or partially filled with liquid at a level below the entrainment onset point. With a sufficient liquid injection, however, the hot leg maintains a certain liquid level and the liquid injection rate are balanced by the boiloff rate plus the entrainment rate. A steady two-phase mixture flow through the branch is expected Fig. 3.3.

The three distinct cases above illustrate that phase separation can occur in several ways during the blowdown transient. To obtain a complete understanding of the process, the following factors should be considered:

(1) Flow regime in the hot leg varies from bubbly flow to intermittent or stratified flow, depending on the inlet conditions. Phase separation in the tee junction occurs under the conditions of all flow regimes, and the liquid carryover is much more pronounced in bubbly/intermittent flows than in stratified flow.
(2) The hot leg inlet condition significantly influences the flow in the tee branch due to the disturbances on the liquid surface at the inlet.
(3) The development length from the inlet to the branch may affect the phase separation at the tee junction since the hot leg flow is in various stages of development.
(4) The downstream condition of the tee branch controls the mass extraction rate in the branch, and thus needs to be examined.

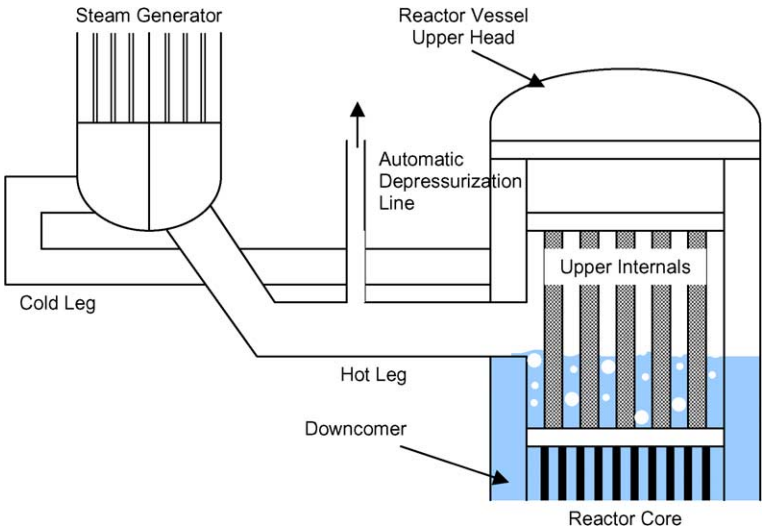

Fig. 3.3. Loss-of-coolant accident sequence or plant blowdown. Final steady-state condition. No liquid injection.

3.2. Facility scaling

With the emphasis on the phase separation phenomena in a horizontal tee with a vertical-up tee branch, the separate effect tests should focus on acquiring data applicable to the prototypic geometry, initial, and boundary conditions. To determine the range of conditions for phase separation, the Westinghouse new pressurized water reactor vessel/hot leg/depressurization line system was used as a reference case. The associated scaling criteria are presented below. The results of the scaling analyses have been omitted due to the proprietary nature of the Westinghouse reactor design.

3.2.1. Hot leg flow condition

According to Zuber (1980), the flow regime in a horizontal duct can be characterized by a plot of the relative liquid height against the Froude number of the vapor phase

$$Fr_G = \frac{j_G\sqrt{\rho_G}}{\sqrt{g\Delta\rho D}} = f\left(\frac{H_L}{D}\right), \tag{3.1}$$

where Fr_G is the vapor phase Froude number, j_G is the superficial gas velocity, ρ_G is the gas density, $\Delta\rho$ is the difference between the liquid and gas densities, g is the gravitational constant, D is the mainline diameter, and H_L is the liquid level in the mainline. For geometric similarity of separated flows, equality of void fraction is

$$\left(\frac{H_L}{D}\right)_m = \left(\frac{H_L}{D}\right)_p, \tag{3.2}$$

where 'm' represents the model and 'p' represents the prototype, respectively. Consequently, the flow regime transitions scale with the vapor Froude number. This provides the ability to easily plan experiments in the stratified, annular, and intermittent flow regimes. To include the bubbly flow case that may occur in the first stage of the automatic depressurization process, the liquid flow rate should be considered. According to Taitel et al. (1977), the flow regime transition from intermittent flow to bubbly flow occurs when turbulent fluctuations are strong enough to overcome the buoyant forces tending to keep the vapor phase at the top of the pipe. The criterion is given by

$$\left\{\frac{|(dp/dx)^s_L|}{g\Delta\rho}\right\} = \left\{\frac{\frac{4}{D}f_L\frac{\rho_L j_L^2}{2}}{g\Delta\rho}\right\} = \{2f_L Fr_L^2\} \geqslant f\left(\frac{H_L}{D}\right), \tag{3.3}$$

where dp/dx is the pressure gradient in the x-direction, f_L is the single-phase coefficient of friction of the liquid, j_L is the superficial liquid velocity, and Fr_L is the liquid Froude number. For turbulent flows with an approximately constant friction factor, this criterion implies that the bubbly/intermittent flow transition boundary is a single line in a plot of the relative liquid height against the Froude number of the liquid phase. With geometric similarity, the flow regime transition scales with the liquid phase Froude number equality.

Essentially, the Froude number scaling criterion is used to preserve the flow regimes and flow conditions. It requires geometric similarity, which generally applies to tee shape and size for fully developed flows. For applications to two-phase flows in a reactor hot leg, especially for the behavior at the branch location, the inlet condition and the developing length to the vertical tee branch should be scaled. As discussed previously, due to the disturbed surface of the two-phase mixture level in the vessel, liquid slugs may form at the hot leg inlet even for the flow that is supposed to be categorized as stratified. Because of the short distance to the tee branch, the liquid slugs would be driven into the branch line, resulting in a significant liquid carryover rate. Conventional experiments feature a uniform mixture inlet and may not be applicable to the actual case. Accordingly, the following geometric groups should be scaled:

$$\text{Void fraction in the vessel: } (\alpha_{\text{Vessel}})_{\text{m}} = (\alpha_{\text{Vessel}})_{\text{p}}, \tag{3.4}$$

$$\text{Hot leg size versus vessel size: } \left(\frac{D_{\text{Hotleg}}}{D_{\text{Vessel}}}\right)_{\text{m}} = \left(\frac{D_{\text{Hotleg}}}{D_{\text{Vessel}}}\right)_{\text{p}}, \tag{3.5}$$

$$\text{and ADS-4 branch location: } \left(\frac{L_{\text{Hotleg/Tee}}}{D_{\text{Hotleg}}}\right)_{\text{m}} = \left(\frac{L_{\text{Hotleg/Tee}}}{D_{\text{Hotleg}}}\right)_{\text{p}}, \tag{3.6}$$

where α_{Vessel} is the void fraction in the reactor vessel, D_{Hotleg} is the hot leg diameter, $L_{\text{Hotleg/Tee}}$ is the horizontal length from the hot leg inlet to the branch, and D_{vessel} is the reactor vessel diameter.

3.2.2. Tee branch flow condition

If the flow in the hot leg is stratified, based on the entrainment model for vertical tee branch flows (Zuber, 1980; Smoglie, 1984; Schrock et al., 1986), the entrainment onset and the entrainment fraction is dependent on the following criterion:

$$Fr_{\text{G}} = \frac{j_{\text{G3}}\sqrt{\rho_{\text{G}}}}{\sqrt{g\Delta\rho D}} \geqslant K\left(\frac{h_{\text{b}}}{D}\right)^{m}\left(\frac{D}{d}\right)^{n}, \tag{3.7}$$

where j_{G3} is the superficial gas velocity in the branch, D is the mainline diameter, d is the branch diameter, and K, m, and n are experimentally determined constants. If the geometric similarity is observed, this criterion implies the equality of the Froude number based on the gas phase superficial velocity in the branch and the hot leg. Along with this entrainment criterion, Reyes (Wilson et al., 1997) proposed using the Kutadeledz number to scale the vertical-up branch due to the consideration of the possibility of flow reversal in large vertical pipes.

$$Ku = \frac{j_{\text{G}}}{\sqrt{(g\sigma\Delta\rho)}^{1/2}/\rho_{\text{G}}} > Ku_0, \tag{3.8}$$

where j_{G} is the superficial gas velocity in the vertical pipe, σ is the surface tension, and Ku_0 is the value of the Kutadeledz number at which flow reversal will begin.

3.2.3. Test conditions

Using liquid and gas flow rates as the control parameters, steady-state tests need to be performed to provide detailed information on the relation between the gas discharge rate and the liquid carryover rate through the vertical branch. Each of the steady-state tests corresponds to one instantaneous point in the blowdown transient. In addition, the AP600 blowdown transient is very fast and the plant will become fully depressurized or just above atmospheric pressure for the large portion of the steady-state entrainment. Hence, 138 kPa is the target reference pressure for the prototypic system. Following the proposed scaling criteria, the following test conditions are identified.

The vessel void fraction at the hot leg inlet elevation needs to be scaled to preserve the inlet condition of the branch flow according to Eq. (3.4). Using the pool bubbly flow correlation developed by Kataoka and Ishii (1987), the corresponding test vessel conditions can be calculated. The selection of the actual size of the test vessel depended on hot leg flow conditions.

To preserve the pool boiling characteristics inside the vessel, the ratio between the maximum sizes of cap bubbles and the vessel diameter was considered. When the test vessel size is scaled down, it is important to maintain its diameter greater than the maximum cap bubble size. Otherwise, the pool boiling characteristics may not be preserved. Instead, the flow will be chaotic slug/churn flow with large fluctuations in pressure and flow rates. The maximum cap bubble size is given by Ishii and Kojasoy (1993):

$$D_{\mathrm{cap,max}} = 40\sqrt{\frac{\sigma}{g\Delta\rho}}. \tag{3.9}$$

At a system pressure of 137.9 kPa, the maximum cap bubble size in the prototypic system is about the same as in the model system, roughly 10 cm in diameter, substantially smaller than the prototypic vessel size.

Flow regime scaling is the most important when the hot leg inlet is submerged in the two-phase mixture. As discussed earlier, initially the flow regime in the prototypic hot leg is most likely dispersed bubbly flow.

When the reactor vessel mixture level is below the upper edge of the hot leg inlet, the flow in the hot leg is most likely in the regimes of stratified flow, intermittent flow, and/or annular flow. According to Eq. (3.1), if geometric similarity is satisfied, the key parameter for hot leg scaling is the two-phase Froude number, which essentially provides a measure to the intermittence. This nondimensional number is the ratio of inertia force to gravity force acting on the liquid surface. When the inertia force (unstable factor) overtakes the gravity force (stable factor), the surface intermittence increases, and therefore the liquid is more vulnerable to being transported to the upper portion of the duct, resulting in significant liquid carryover to the vertical-up branch in the hot leg.

The gas flow rate in the branch depends on the break size and location. In most cases, vapor will be extracted by the branch unless a large break occurs in the hot leg. Assuming that half of the boiloff steam is released from one branch at 137.9 kPa which is the target reference pressure, the gas superficial velocity in the prototypic branch ranges from 22 m/s to 170 m/s for a decay power of 0.5–2% of the full power. From the flow regime map for vertical

pipe flows, the two-phase flow in the prototypic branch should be in the annular flow regime. This conclusion is further justified by the annular flow regime transition criterion (Todreas and Kazimi, 1988)

$$Ku \geqslant 3.1. \tag{3.10}$$

4. Experimental methods

The Air–water Test Loop for Advanced Thermal–hydraulic Studies (ATLATS) separate- effects test facility shown in Fig. 4.1 was modeled after the Westinghouse AP600 reactor. A scaling analysis was completed to determine appropriate pipe and vessel sizing to ensure preservation of the entrainment phenomenon. During the postulated accident condition outlined in the Scaling section, most of the liquid entrainment occurs after the plant has quickly depressurized to atmospheric conditions. In addition, the analysis by Schrock et al. indicated little difference between air–water and steam–water results. Air and water were chosen as the working fluids to allow a more economical test plan.

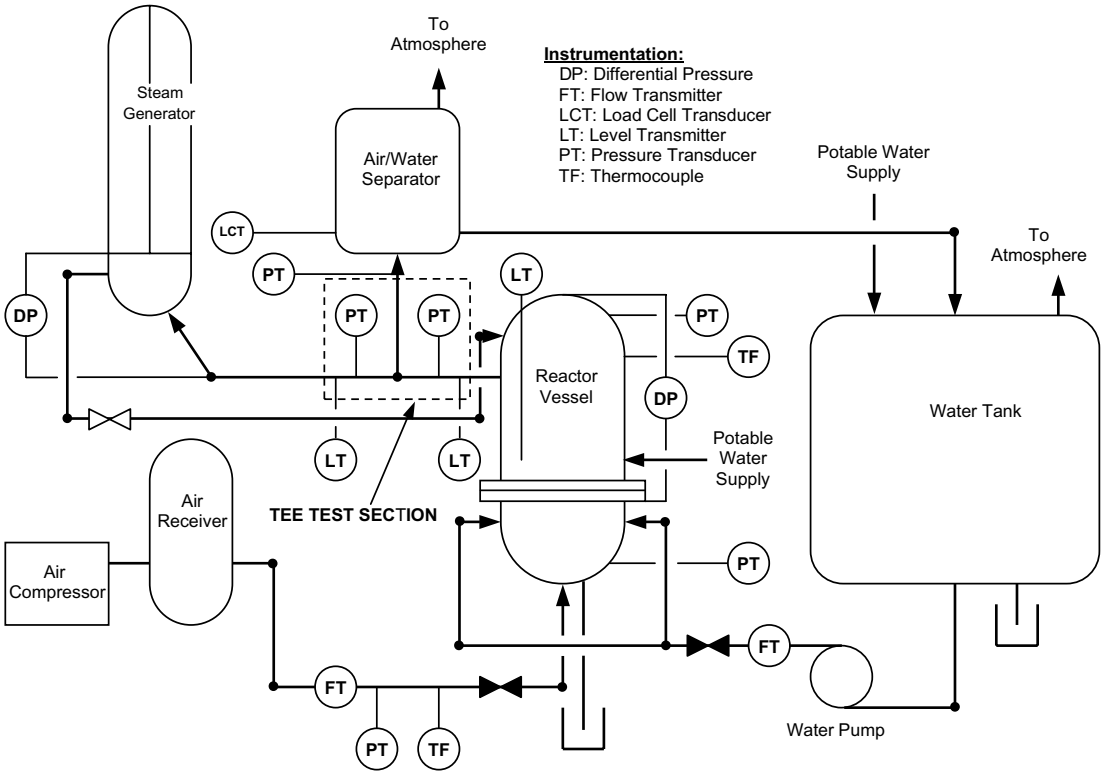

Fig. 4.1. Air–water Test Loop for Advanced Thermal–hydraulic Studies (ATLATS).

Air flow was provided in ATLATS at atmospheric pressure by a large air compressor connected to the reactor vessel lower head of the reactor vessel. Water was injected using a water pump connected to the sides of the lower head. Air flowed from the lower head through seven porous tubes into the core region of the vessel to simulate decay heat boiling. The tee test section was made from clear PVC rated at 138 kPa gauge to allow visual recording of the hot leg entrainment phenomenon. View ports on the side and top of the reactor vessel provided a view into the simulated boiling in the core region. The tee test section outlet led to a model steam generator constructed from steel and clear Tygon tubing. In some cases, a return line was added to the cold leg side of the steam generator leading back to the reactor upper head. This return line was used to normalize the pressure on both sides of the tee.

4.1. Instrumentation

Fig. 4.1 shows the locations of all ATLATS instrumentation. Critical instrumentation included the two hot leg half-ring-type impedance probes (LTs on the test section in Fig. 4.1), inlet air and water flow meters, test section thermocouples and pressure sensors, and reactor vessel mixture and collapsed liquid level probes.

Fig. 4.2 is an illustration of the half-ring type impedance probe developed at Oregon State University (OSU) for measuring of the two-phase stratified liquid level in the hot leg. Two sets of probes were installed upstream and downstream of the vertical tee branch. The probes were constructed from two 14 gauge stainless steel wires flush-mounted on the inside periphery of a section of PVC ring that was sandwiched between two flanges. By measuring the impedance in the stratified flow, the water level in the horizontal duct was obtained. A sine wave oscillator provided a

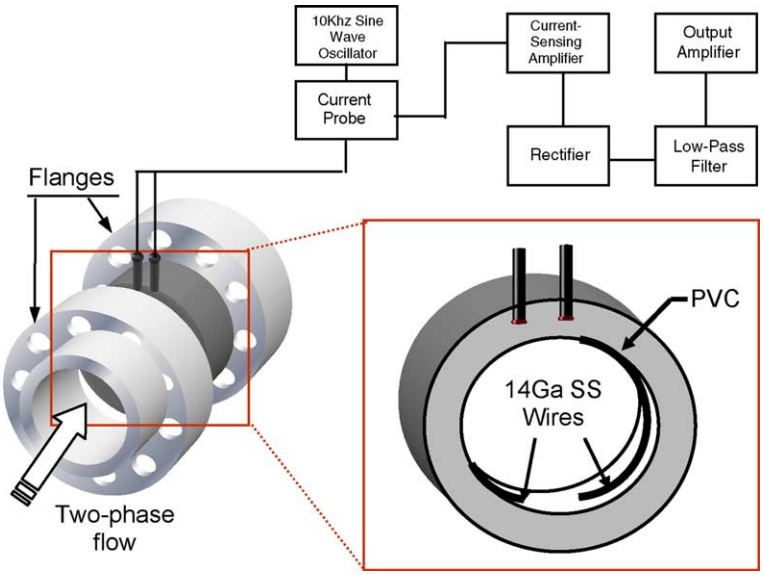

Fig. 4.2. Half-ring-type impedance probe.

10 kHz signal to the water through the two wire electrodes at a regulated voltage. The current draw from the probe was sent to a current-sensing amplifier. This signal was rectified and filtered to remove high frequency noise, and eventually was amplified to provide a voltage output from 2 to 9 volts.

Because the distance between the two wire electrodes increases as the water level rises, nonlinear voltage response to the water level was expected. Each probe was calibrated using water level measurements from the reactor vessel differential pressure sensor. Before each test, the probes were calibrated to reduce measurement drift due to impurities in the working fluid.

There are two main sources of uncertainty in the measurements: instrument calibration and data acquisition circuitry. These uncertainties are additive and their resulting total uncertainty can be expressed by the common propagation-of-error equation for small measured uncertainties. The largest uncertainty was associated with measuring the hot leg level using the two impedance probes, which can be as high as 9% full range. All other instrument measurement uncertainty was below 5% full range.

The transparent tee test-section, steam generator tubes, and reactor view ports enabled VHS recording of the phase separation phenomenon. For more detailed examination of the hot leg entrainment phenomenon, a high-speed camera system was used. This enabled recording of up to 500 frames per second for up to 4 seconds. Slow playback of the high-speed films gave startling results about the structure of the two-phase flow in the hot leg during liquid entrainment.

4.2. Test procedures

Over 100 separate-effects tests were run during a three-year period in ATLATS. The tests can be split into two main categories: onset of entrainment (blowdown without liquid injection) and steady-state entrainment (blowdown with liquid injection). The procedures for these two categories of tests are described below.

4.2.1. Onset entrainment test procedures

The objectives of the entrainment onset test were to determine the liquid level in the hot leg when liquid entrainment to the branch occurred at a specified gas flow rate. The volumetric airflow rate ranged from 0.028 m^3/s to 0.34 m^3/s, corresponding to air velocities of about 15–170 m/s at the branch exit. In the hot leg, air superficial velocity ranged from 1.4 m/s to 16 m/s. The entire system was slightly pressurized to 41.4 kPa gauge.

Two approaches were taken to determine the entrainment onset condition. The direct approach was to visualize the onset of liquid entrainment while changing the airflow rate. However, due to the unsteady level in the reactor vessel, irregular surface waves propagated to the branch location, making the task extremely challenging. The second approach was to find the liquid level when entrainment stops at a given gas flow rate as shown in Fig. 4.3.

Initially, the test vessel was filled with water above the hot leg opening (Fig. 4.3a) and then airflow was provided at a prescribed flow rate. Liquid entrainment through the branch followed (Fig. 4.3b and c) and finally stopped (Fig. 4.3d) when the water level in the hot leg reached a critical height. This approach required an airflow velocity in the branch exceeding the limit of flow rever-

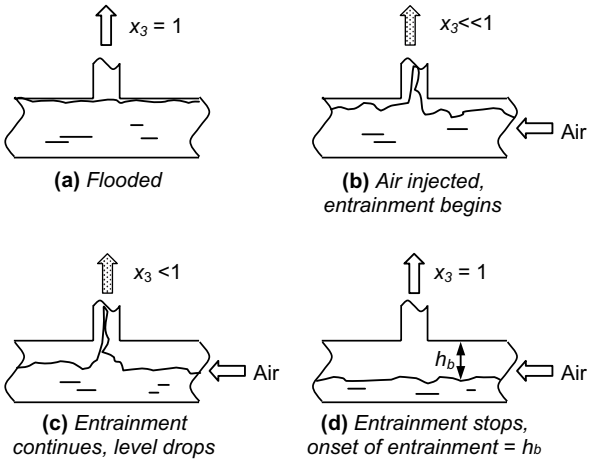

Fig. 4.3. Entrainment onset two-phase flow structure.

sal, which in fact was true for the flow conditions of interest. Indeed, the branch size was scaled to guarantee the preservation of the onset phenomenon.

4.2.2. Entrainment rate test procedures

The purpose of the entrainment rate tests was to measure the steady-state liquid level in the hot leg for a given gas and liquid flow rate. Therefore, these tests were conducted as a series of steady-state steps or points. Flow conditions for the experiments were selected based on the scaling analyses to collect data most of which pertained to the transition and slug or intermittent flow regimes. The liquid superficial velocity in the vertical-up depressurization line varied from 0.155 m/s to 1.87 m/s and the air superficial velocity from 11.6 m/s to 140 m/s. For flow in the hot leg, the superficial liquid velocity ranged from 0.017 m/s to 0.208 m/s and the air superficial velocity from 1.29 m/s to 15.5 m/s. The reactor vessel was filled relatively full with water and a specific gas flow was throttled. The simulated decay boiling created a churning two-phase mixture in the vessel. Then the liquid was throttled to a specified rate. The mixture level in the vessel rose and filled the hot leg, eventually passing the onset level. At this point, steady-state entrainment was achieved. The time was recorded and this steady-state point was held for approximately 5 minutes. After enough data were collected, the liquid flow was throttled to a slightly higher flow rate, and another steady-state data point was obtained. This procedure was repeated for several different liquid flow rates for one gas flow rate.

5. Results

The experimental results are presented in two sections: onset of entrainment and steady-state entrainment rate. Observations were recorded visually using a high-speed camera and are

accompanied by illustrations to help describe the phenomenon. Nondimensional data is presented in tabular form and, in some cases, plotted to aid discussions.

5.1. Onset of entrainment

The two-phase flow structure in hot leg at the onset of liquid entrainment was recorded visually as stratified or stratified-wavy. Surface instabilities were created by the violent fluctuations in the reactor vessel mixture level and propagated through the hot leg and were reflected back by the downstream pressure boundary (steam generator inlet pipe). At high gas flow rates the shearing between the gas and liquid phase also contributed to surface instabilities. Previous studies by Schrock et al. and Reimann attempted to maintain a quiescent stratified interface using a mixing tee.

Table 5.1
ATLATS entrainment onset data

P (Pa)	T (C)	w_{G3} (kg/s)	h_b/D
102,071	13.60	0.0364	0.239
102,596	20.61	0.0552	0.293
102,619	25.91	0.0684	0.396
104,089	26.96	0.0907	0.391
106,045	26.88	0.1134	0.463
107,432	28.41	0.1279	0.475
108,907	28.54	0.142	0.505
112,047	28.13	0.1702	0.54
115,589	28.29	0.1984	0.577
118,788	29.23	0.2253	0.645
124,213	29.30	0.2569	0.643
129,527	29.41	0.2843	0.634
102,787	13.2	0.029	0.215
103,780	12.9	0.0589	0.255
105,021	12.6	0.0839	0.317
106,696	12.3	0.1117	0.423
109,420	12.1	0.1428	0.452
112,660	12	0.1723	0.488
116,039	11.9	0.2012	0.517
120,383	11.9	0.2307	0.543
122,658	12	0.2505	0.602
128,794	12.1	0.2856	0.608
132,655	12.1	0.3083	0.62
139,826	12.4	0.3452	0.612
103,463	9.22	0.0315	0.215
103,718	9.16	0.064	0.335
104,752	8.99	0.085	0.445
107,048	8.85	0.1179	0.493
109,351	8.71	0.1417	0.497
112,178	8.71	0.1683	0.518
116,108	8.82	0.2012	0.552
120,245	9.23	0.2312	0.592
126,312	9.73	0.2573	0.583

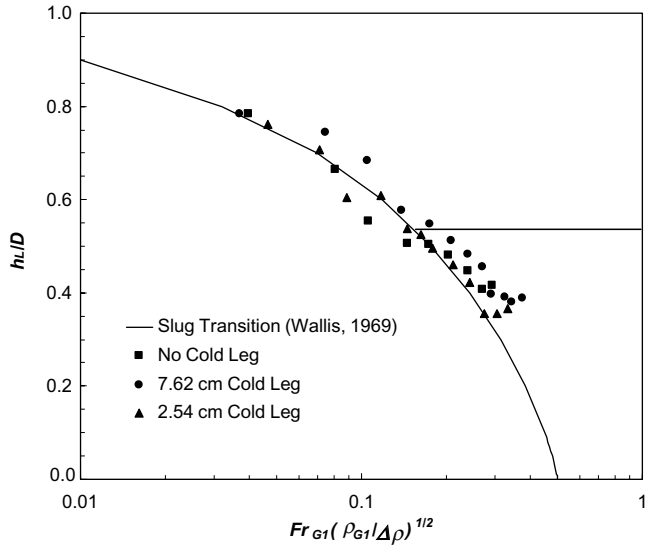

Fig. 5.1. ATLATS entrainment onset data.

However, this experimental approach was not consistent with the full range of flow conditions for a prototypic facility under accident conditions.

The onset data in Table 5.1 is plotted in Fig. 5.1 as h_L/D (where $D = h_b + h_L$) versus the Froude number times a density ratio. It was interesting to plot ATLATS onset data against the slug transition line (Wallis, 1969), since the graph illustrates that the onset phenomenon in a horizontal pipe with a vertically-up branch is quantitatively similar to a slug forming in a horizontal pipe. Also plotted in Fig. 5.1 is the variation of onset level versus modifications in the size of the downstream cold leg, which is located on the outlet of the steam generator. This effectively varies the downstream line resistance in a way that corresponds to different stages of steam generator tube draining during an LOCA. From Fig. 5.1, it seems that the downstream flow resistance through the steam generator has little effect on the onset of entrainment height. Later in this article, ATLATS data will be compared to other data sets along with currently available onset correlations.

5.2. Entrainment rate

The most notable characteristic of steady-state liquid entrainment in ATLATS is the presence of an oscillatory slug between the vertical branch and steam generator inlet (illustrated in Fig. 5.2). Previous entrainment studies relied on developed flow with long ranges of pipe on either side of the branch to diminish surface instability effects. While this approach proved effective in obtaining entrainment data in the stratified flow regime, it is not applicable for the entire range of prototypic accident conditions.

The flow regime encountered in the ATLATS hot leg was much different then fully developed two-phase flow in a horizontal pipe. Intuitively, the presence of a vertical branch should increase

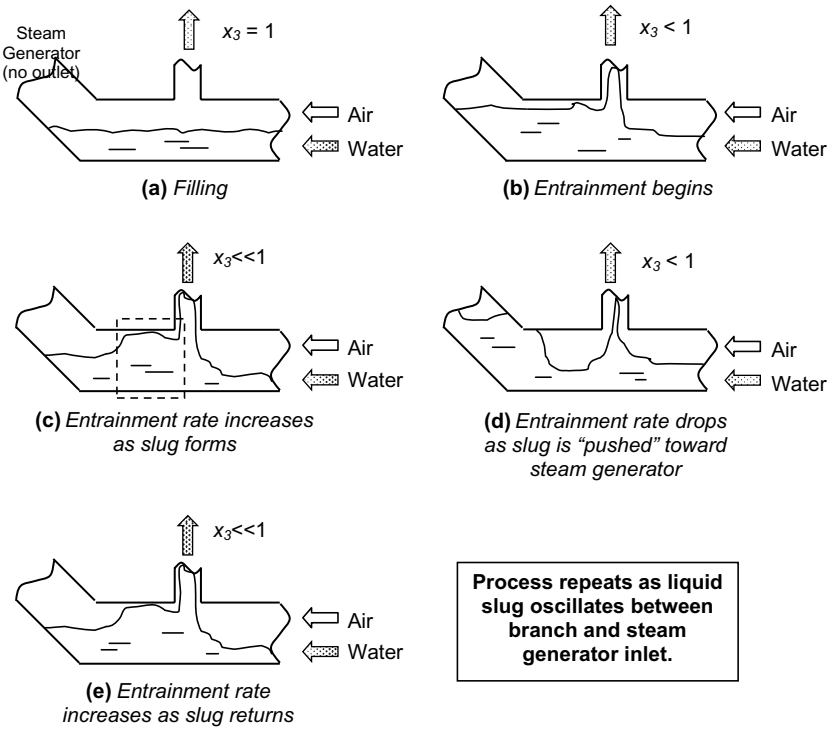

Fig. 5.2. Steady-state entrainment rate two-phase structure for intermittent flow.

the tendency for the liquid surface to become unstable and jump to the top of the pipe, thus altering the stratified-to-slug transition criterion. In addition, the oscillatory water slug observed in

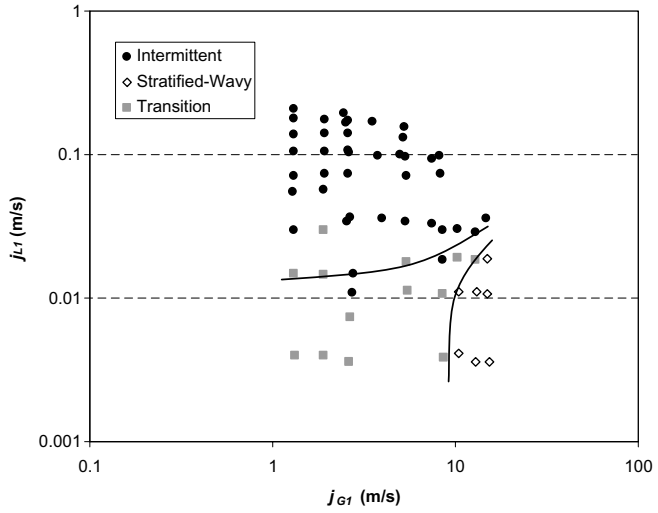

Fig. 5.3. Flow regime mapping of ATLATS entrainment rate data in the reactor hot leg.

Table 5.2
ATLATS entrainment rate data

T (C)	P (Pa)	w_{G3} (kg/s)	w_{L3} (kg/s)	h/D	h_b/D	x_3	Flow regime[a]
13.70	127,001	0.037	3.772	0.227	0.194	0.010	INT
13.70	123,278	0.036	3.262	0.247	0.192	0.011	INT
13.70	119,348	0.034	2.519	0.258	0.190	0.013	INT
13.60	115,970	0.033	1.914	0.259	0.189	0.017	INT
13.00	112,040	0.032	1.297	0.256	0.187	0.024	INT
12.10	110,109	0.032	0.995	0.253	0.185	0.031	INT
12.10	107,124	0.031	0.543	0.226	0.185	0.054	INT
12.20	105,055	0.031	0.269	0.205	0.184	0.102	TR
12.30	103,690	0.031	0.072	0.235	0.185	0.297	TR
15.11	126,313	0.053	3.198	0.274	0.243	0.016	INT
13.70	121,794	0.052	2.559	0.280	0.241	0.020	INT
13.70	117,941	0.050	1.901	0.284	0.239	0.026	INT
13.48	114,299	0.048	1.345	0.296	0.237	0.035	INT
12.60	111,833	0.047	1.033	0.293	0.235	0.044	INT
12.80	108,006	0.046	0.545	0.261	0.232	0.077	TR
13.30	105,297	0.044	0.266	0.259	0.231	0.143	TR
13.60	103,821	0.044	0.073	0.263	0.229	0.374	TR
20.85	132,387	0.070	3.532	0.217	0.282	0.019	INT
20.85	129,004	0.070	3.041	0.223	0.286	0.023	INT
14.85	128,941	0.074	3.143	0.257	0.292	0.023	INT
16.15	123,961	0.070	2.544	0.258	0.288	0.027	INT
16.09	120,091	0.068	1.959	0.272	0.285	0.034	INT
20.85	120,579	0.068	1.887	0.328	0.285	0.035	INT
15.33	115,652	0.066	1.333	0.308	0.282	0.047	INT
20.85	109,836	0.060	0.624	0.295	0.273	0.088	INT
9.57	110,324	0.066	0.663	0.262	0.285	0.091	INT
9.37	106,569	0.066	0.270	0.263	0.287	0.196	INT
9.84	105,760	0.064	0.197	0.230	0.284	0.246	INT
10.17	105,158	0.062	0.133	0.219	0.279	0.318	TR
10.77	104,270	0.061	0.066	0.255	0.277	0.482	TR
11.17	137,052	0.108	3.110	0.282	0.357	0.034	INT
20.85	124,601	0.101	1.797	0.289	0.354	0.053	INT
20.85	144,846	0.163	2.815	0.269	0.438	0.055	INT
14.22	137,853	0.157	2.376	0.300	0.433	0.062	INT
15.98	129,677	0.142	1.835	0.326	0.417	0.072	INT
20.85	132,791	0.151	1.763	0.302	0.431	0.079	INT
15.31	124,347	0.147	1.304	0.324	0.430	0.101	INT
20.85	112,788	0.096	0.654	0.348	0.353	0.128	INT
20.85	118,728	0.137	0.619	0.407	0.421	0.181	INT
9.67	113,613	0.138	0.324	0.415	0.423	0.298	TR
9.52	111,703	0.137	0.207	0.416	0.423	0.398	TR
19.85	145,915	0.236	1.712	0.328	0.524	0.121	INT
14.85	145,624	0.262	1.789	0.365	0.548	0.128	INT
15.08	138,537	0.251	1.349	0.372	0.543	0.157	INT
20.85	127,679	0.206	0.605	0.433	0.507	0.254	INT
9.90	127,914	0.244	0.546	0.533	0.544	0.309	INT
9.68	122,931	0.235	0.338	0.525	0.539	0.410	INT
9.99	120,245	0.230	0.196	0.499	0.537	0.540	TR

(*continued on next page*)

Table 5.2 (*continued*)

T (C)	P (Pa)	w_{G3} (kg/s)	w_{L3} (kg/s)	h/D	h_b/D	x_3	Flow regime[a]
9.96	117,014	0.225	0.070	0.494	0.535	0.763	TR
10.01	134,818	0.310	0.553	0.604	0.598	0.359	INT
9.77	133,800	0.308	0.346	0.580	0.597	0.471	TR
10.13	129,505	0.300	0.203	0.581	0.595	0.597	SW
10.17	122,565	0.286	0.075	0.620	0.589	0.793	SW
9.98	150,786	0.432	0.520	0.605	0.668	0.454	INT
9.71	146,158	0.420	0.335	0.620	0.665	0.556	TR
10.10	139,121	0.407	0.203	0.635	0.664	0.667	SW
10.28	130,596	0.377	0.066	0.682	0.652	0.851	SW
12.40	158,969	0.516	0.650	0.611	0.707	0.443	INT
9.73	157,562	0.528	0.343	0.645	0.714	0.606	SW
10.27	147,565	0.491	0.195	0.672	0.704	0.716	SW
10.41	140,277	0.479	0.065	0.720	0.704	0.880	SW

[a] INT = Intermittent, SW = Stratified-Wavy, TR = Transition.

ATLATS had no outlet and became "trapped" due to the inclined steam generator inlet. Consequently, this was not the conventional "slug" flow regime encountered in developed horizontal pipes, but one that is unique to the ATLATS/AP600 design.

In this study, two unique flow regimes were defined: stratified-wavy-to-intermittent transition and intermittent and are mapped in Fig. 5.3. The data are listed in Table 5.2.

6. Theoretical modeling

The modeling of liquid entrainment in a tee junction with an upward oriented branch was traditionally carried out in two steps. First, when entrainment begins, the gas chamber height h_b in the horizontal pipe is calculated from a critical gas/vapor flow rate w_{G3} through the branch as shown in Fig. 1.2. When the actual liquid level in the horizontal pipe is higher than the critical level (i.e. $h < h_b$) liquid entrainment begins. In the second step the onset level predicted from the gas flow rate, along with the actual level measured, is used to determine the branch gas flow quality x_3. In this study, the proposed model follows the same two-step convention.

6.1. Entrainment onset criterion

The proposed model starts from the semiempirical correlation of Maciaszek and Micaelli (1986) Their analysis was based on an approach considered by Bharathan et al. (1982) for liquid entrainment in a container with a relatively large break. Essentially the model relies on the interface instability under the opening as shown in Fig. 6.1. According to Maciaszek and Micaelli (1986) when gas flows into the branch, a postulated ring-shape wave can form under the opening. As the gas flow through a cylinder of a diameter equal to the wave separation reaches a critical value, it is assumed that the wave can grow without bound, resulting in liquid entrainment. This is sim-

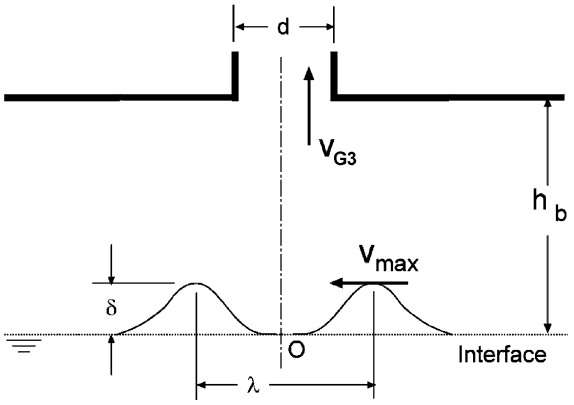

Fig. 6.1. Surface instabilities associated with the onset of liquid entrainment.

ilar to the slug transition experienced in a horizontal pipe. Different from liquid droplet entrainment in annular flows, liquid viscosity and surface tension play a relatively minor role on the growth of the wave, and thus are eliminated in the modeling. Based on this rationale, a wave of height δ and spacing λ is considered, which leads to the following continuity equation for the gas flow over the wave crest:

$$\rho_G v_{max}(\pi\lambda)(h_b - \delta) \approx \rho_{G3} v_{G3} \frac{\pi d^2}{4} = w_{G3}, \tag{6.1}$$

where v_{max} is the gas velocity at the top of the wave (Fig. 6.1), v_{G3} is the gas velocity in the branch, and w_{G3} is the mass gas flow rate in the branch. Without considering the kinetic energy of liquid far from the branch opening, the change in pressure from the wave crest to the stagnation point is found to be:

$$\Delta p = \Delta\rho g\delta = \frac{1}{2}\rho_G v_{max}^2 \tag{6.2}$$

where p is the pressure and v_{max} is the same as in Eq. (6.1). Substituting Eq. (6.2) into Eq. (6.1) results in

$$\lambda^2\delta(h_b - \delta)^2 = \frac{w_{G3}^2}{2\pi^2\rho_G\Delta\rho g}. \tag{6.3}$$

This equation contains the critical gas flow rate w_{G3} and the gas chamber height h_b for entrainment onset. The unknown parameters are the wave height δ and spacing λ. For any given gas mass flow rate, if the wave spacing is only a function of h_b, which is true from the potential flow analysis described later, the change of wave height with respect to h_b can be obtained:

$$\frac{\partial\delta}{\partial h_b} = \frac{2\delta(\delta - h_b)}{h_b^2 - 4h_b\delta + 3\delta^2}, \tag{6.4}$$

where ∂d and ∂h_b are the partial derivatives of δ and h_b, respectively. When the change in δ with respect to h_b approaches infinity, entrainment begins, leading to the critical wave height equal to

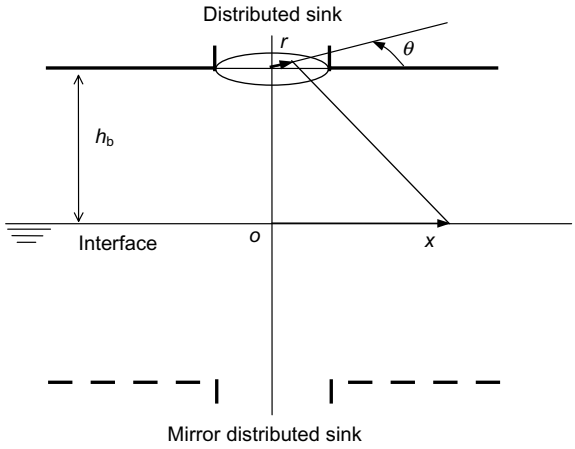

Fig. 6.2. Potential flow model for gas velocity.

one-third of h_b. Substituting the critical wave height into Eq. (6.3) and solving for the corresponding gas chamber height, the liquid entrainment onset criterion becomes:

$$h_b = \frac{3}{2}\left(\frac{w_{G3}^2}{\pi^2 \rho_G \Delta\rho g \lambda^2}\right)^{1/3}. \tag{6.5}$$

If the wave spacing λ is assumed to be the same as the branch diameter, Eq. (6.5) is reduced to the liquid entrainment onset correlation of Maciaszek and Micaelli (1986) with an adjustable experimental factor of 0.88.

Generally, λ should be a function of the branch size and the location of the interface. This is because the wave crest should appear where the gas pressure over the interface is minimum, corresponding to a maximum gas velocity. To take this phenomenon into consideration, a potential flow analysis is proposed to identify the wave crest separation.

By neglecting gas viscosity under a steady-state condition, potential flow theory is applicable by considering the gas flow field as the result of two distributed sinks located at opposite sides of the interface, as demonstrated in Fig. 6.2. The distributed sink above the interface is the actual branch inlet, whereas the mirrored sink below the interface represents an imaginary sink needed to satisfy the boundary condition at the interface when the sidewall confinement effect is neglected. Assuming a uniform velocity distribution across the branch inlet and employing a coordinate system defined in Fig. 6.2, the gas velocity over the gas-liquid interface can be expressed as the superposition of the flow fields caused by the two distributed sinks:

$$v_x = \left(\frac{4w_{G3}}{\pi^2 \rho_G d^2}\right) \int_0^{d/2} \int_0^{2\pi} \frac{(x - r\cos\theta)}{[h_b^2 + (r\sin\theta)^2 + (x - r\cos\theta)^2]^{3/2}} r\,d\theta\,dr, \tag{6.6}$$

where v_x is the velocity in the x-direction, r is the radius of the potential sink, and θ is the angle of the radius r with respect to the coordinate axis. The dimensionless form of this equation is given by

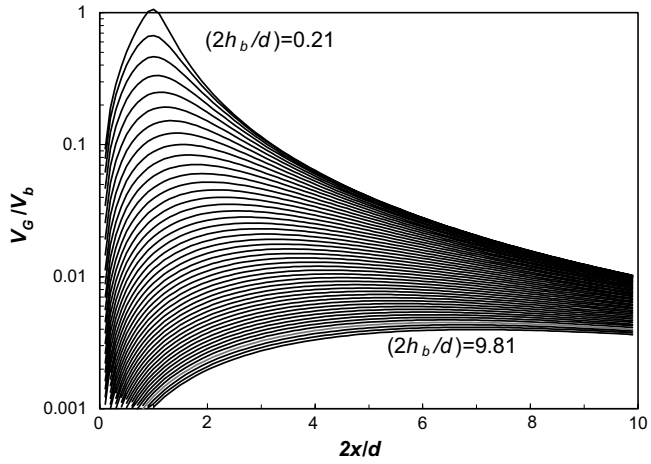

Fig. 6.3. Gas velocity distribution along the interface.

$$v_x^* = \frac{v_x}{[w_{G3}/(1/4\pi d^2 \rho_G)]} = \frac{v_x}{v_b} = f(x^*, h_b^*), \tag{6.7}$$

where v_b is the average gas velocity at the branch inlet. The dimensionless groups are defined as:

$$x^* = \frac{x}{(d/2)} \quad h_b^* = \frac{h_b}{(d/2)} \quad \text{and} \quad r^* = \frac{r}{(d/2)}. \tag{6.8}$$

The function, $f(x^*, h_b^*)$, can be solved numerically in terms of x^* and h_b^* and is graphed in Fig. 6.3, which provides the velocity profile along the interface as the interface level changes. As expected, for each fixed gas chamber height h_b there is a maximum v_x where the wave crest is located and liquid entrainment occurs. Fig. 6.4 is a graph of the dimensionless wave spacing $2\lambda/d$ as a function of the dimensionless inception height h_b^*. As the interface level approaches the branch

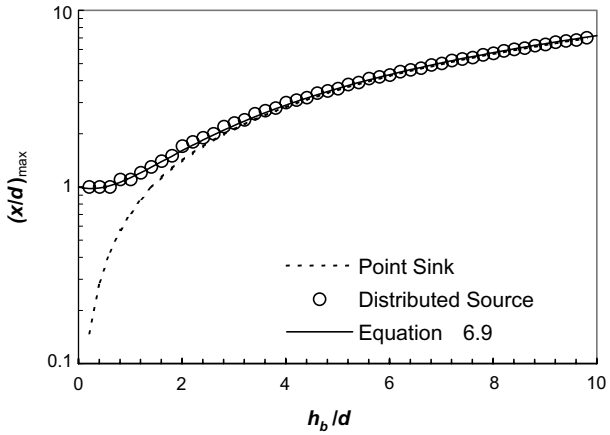

Fig. 6.4. Wave crest spacing versus h_b/d.

inlet, the wave crest moves towards the branch opening. However, the wave crest cannot go farther inward than the branch opening boundary. Hence, the wave spacing is limited by the branch diameter d. On the other hand, when the branch size decreases or the interface level drops, the wave spacing approaches a simple solution $2^{1/2}h_b$ presented in Fig. 6.4 as a dotted line. This is the asymptotic solution of Eq. (6.7) when the branch size shrinks to zero, i.e., a point sink case. It suggests that the wave spacing is independent of the branch size when h_b/d is sufficiently large, corresponding to a condition when the branch size is small compared to the distance from the interface to the branch opening. This corresponds to the correlation developed by Schrock et al. and Reimann and Khan (1994).

Since an analytic solution for λ cannot be found due to the complex nature of the integration in Eq. (6.7), the following simple function is proposed to capture the variation of λ with respect to h_b as well as d.

$$\frac{\lambda}{d} = 0.22\left(\frac{h_b}{d}\right) + 1. \tag{6.9}$$

Substituting Eq. (6.9) into the entrainment onset criterion (Eq. 6.5) leads to the dimensionless solution of the critical gas mass flow rate for the onset of liquid entrainment in a vertical tee junction.

$$\frac{w_{G3}^2}{d^5\rho_G\Delta\rho g} = K\left(\frac{h_b}{d}\right)^3\left[0.22\left(\frac{h_b}{d}\right) + 1\right]^2, \tag{6.10}$$

where K is some constant. To further consider the finite gas velocity far away from the branch, we propose another factor in the following way:

$$\frac{w_{G3}^2}{d^5\rho_G\Delta\rho g} = K\left(\frac{h_b}{d}\right)^3\left[0.22\left(\frac{h_b}{d}\right) + 1\right]^2\left[1 - \left(\frac{h_b}{D}\right)^2\right]^{-1}. \tag{6.11}$$

The theoretical value of the K factor is 0.636 and the best fit to experimental data gives a K of 0.65. The current entrainment onset criterion in the form of Eq. (6.11) agrees with the semiempirical correlations developed in previous studies. When the branch size is relatively small compared to the distance from the interface to the branch opening, Eq. (6.11) reduces to the correlations proposed by Schrock et al. and by Smoglie. For such a condition, the critical gas mass flow rate is independent of the branch size. Similarly, the correlation of Maciaszek and Micaelli (1986) can also be obtained from the new criterion if the branch size is sufficiently large relative to the gas space height, corresponding to the case when λ is approximately equal to d.

6.2. Entrainment rate correlation

When liquid level is above the entrainment onset liquid level, liquid entrainment occurs. Steady-state entrainment of liquid from the horizontal pipe into the vertical branch is difficult to model across multiple flow regimes. This is apparent since the models available to predict branch gas flow quality are empirical curve fits (Table 2.3). In this study, a steady-state first-order approximation is employed by considering time-averaged values in intermittent two-phase flows. By averaging the effects of the two-phase flow intermittency over time domain, a physical model becomes

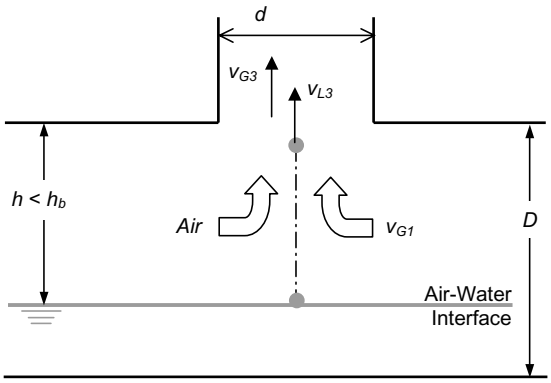

Fig. 6.5. Illustration of steady-state liquid entrainment.

possible. To improve accuracy, higher order terms could be added in the future to include the effects of the large deviations in liquid level. However, additions of higher order terms could be incompatible with the existing system codes (e.g. RELAPs) that rely on the time-averaged two-fluid model.

When liquid is entrained from the horizontal pipe into the branch, the liquid continuum loses its transverse velocity, turns 90 degrees, and continues to travel up the branch. The kinetic and potential energy gain of the entrained liquid should correspond to an energy loss in the gas flow, which is assumed to be proportional to the available gas phase kinetic energy in the horizontal pipe:

$$\frac{1}{2}\rho_{G1}v_{G1}^2 \propto C\Delta\rho gh + \frac{1}{2}\rho_L v_{L3}^2, \tag{6.12}$$

where h is the distance from the average two-phase interface to the branch inlet shown in Fig. 6.5, v_{G1} is the gas velocity in the mainline, v_{L3} is the liquid velocity in the branch, and C is some constant. The adjustable parameter C is used to match the entrainment onset condition, which will be addressed later. Since the only way for fluids to exit the horizontal pipe when a steam generator is installed on the outlet of the mainline is through the branch, the following continuity equations can be applied:

$$w_{G3} = v_{G3}\alpha_3 A_3 \rho_{G3} = v_{G1}\alpha_1 A_1 \rho_{G1} \tag{6.13}$$

and

$$w_{L3} = v_{L3}(1-\alpha_3)A_3\rho_L, \tag{6.14}$$

where α is the void fraction, A is the pipe area, w is the mass flow rate, and v is the velocity for the gas (subscript = G) and liquid (subscript = L) in the hot leg (subscript = 1) and branch (subscript = 3). Substituting these two equations into Eq. (6.12) gives

$$w_{L3} \propto (1-\alpha_3)A_3\sqrt{\frac{C\rho_L}{\rho_{G1}}\left(\frac{w_{G3}}{\alpha_1 A_1}\right)^2 - 2\rho_L\Delta\rho gh}. \tag{6.15}$$

The liquid mass flow rate w_{L3} out the branch is thus related to the gas flow rate w_{G3} out the branch and the gas space height h. The mainline void fraction α_1 can be determined from h, but an appropriate formulation is needed for the branch void fraction α_3. Since void fraction is notoriously difficult to predict, the following simple form is assumed to meet the asymptotic conditions for single-phase liquid and gas flows in the branch:

$$\alpha_3 = \frac{h}{h_b}. \tag{6.16}$$

Eq. (6.15) has to satisfy the newly developed entrainment onset criterion when w_{L3} equals zero as h reaches h_b, which requires that the adjustable parameter C take the following form:

$$C = \frac{0.125\pi^2\left[1-\left(\frac{h_b}{D}\right)^2\right]\left(\frac{D}{d}\right)^4\alpha_{1b}^2}{K\left[0.22\left(\frac{h_b}{d}\right)+1\right]^2\left(\frac{h_b}{d}\right)^2}, \tag{6.17}$$

where α_{1b} is the void fraction in the horizontal pipe at which liquid entrainment begins and is given by:

$$\alpha_{1b} = 1 - \frac{1}{\pi}\cos^{-1}\left[\frac{2h_b}{D}-1\right] + \frac{2}{\pi}\left[\frac{2h_b}{D}-1\right]\left[\frac{h_b}{D}\left(1-\frac{h_b}{D}\right)\right]^{1/2}. \tag{6.18}$$

Finally, the branch gas flow quality x_3 can be readily obtained

$$x_3 = \frac{1}{1+w_{L3}/w_{G3}}, \text{ where} \tag{6.19}$$

$$\frac{w_{L3}}{w_{G3}} = C_1\frac{\left(1-\left(\frac{h}{h_b}\right)\right)\sqrt{\left(\frac{\rho_L h}{\rho_G h_b}\right)\left(1-\left(\frac{h_b}{D}\right)^2\right)\left[\left(\frac{h_b}{h}\right)\left(\frac{\alpha_{1b}}{\alpha_1}\right)^2-1\right]}}{\left(\frac{h_b}{d}\right)\left(0.22\frac{h_b}{d}+1\right)} \tag{6.20}$$

and C_1 is the only experimentally determined constant. This factor is currently set to be 3.0 for best performance of the correlation. The entrainment onset gas chamber height h_b can be readily obtained from Eq. (6.11) for a given gas mass flow rate. It is important to point out that the branch line flow quality does not depend only on h/h_b. Other parameters like the mainline diameter D, branch line size d, and fluid densities are also necessary in determining the branch line flow quality x_3.

7. Comparisons

The correlations in Tables 2.2 and 2.3 and the proposed model (Eqs. 6.11 and 6.19) are compared using test data from the Berkeley (UCB), KfK, and ATLATS test facilities. Some steam–water entrainment onset data were obtained at Berkeley and were lumped with the air–water data since there are no significant differences between the two. The ATLATS data were obtained at

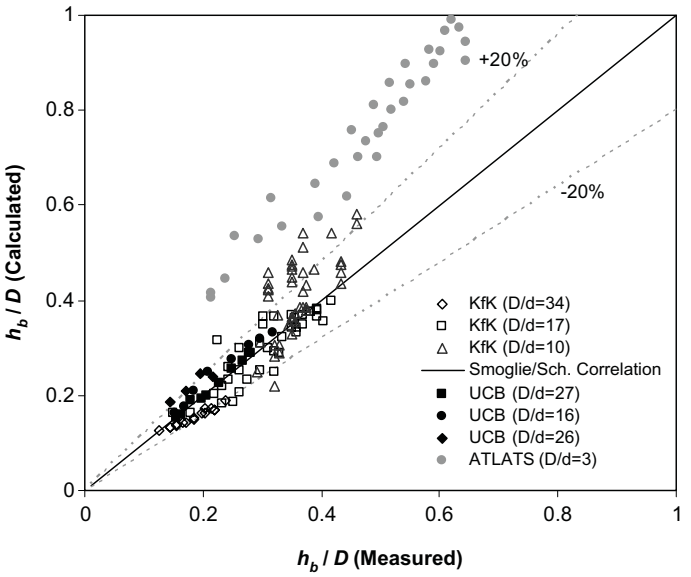

Fig. 7.1. Entrainment onset criterion of Smoglie/Schrock et al. vs. test data.

Oregon State University in an air–water test facility scaled by Wu to the AP600 design (Welter, 2002). Data from CEA (Maciaszek and Micaelli, 1986) was not included because it was published in a form (h/h_{lim}) which could not be reduced to h and h_{b} without making oversimplifying assumptions.

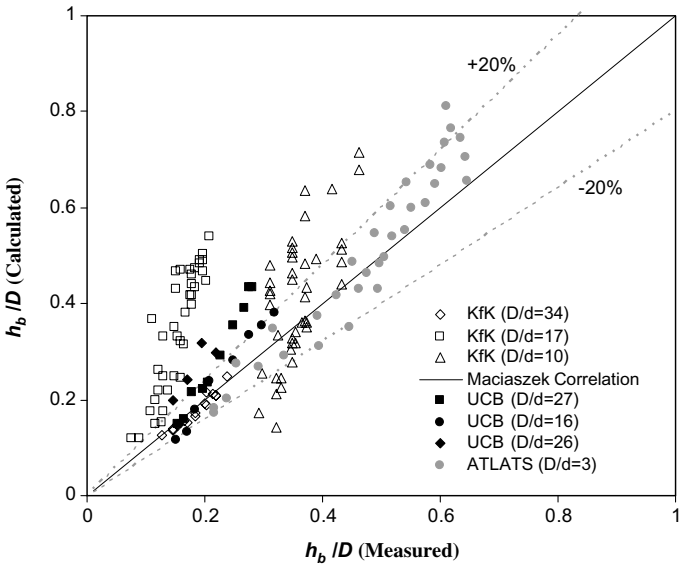

Fig. 7.2. Entrainment onset criterion of Maciaszeck et al. vs. test data.

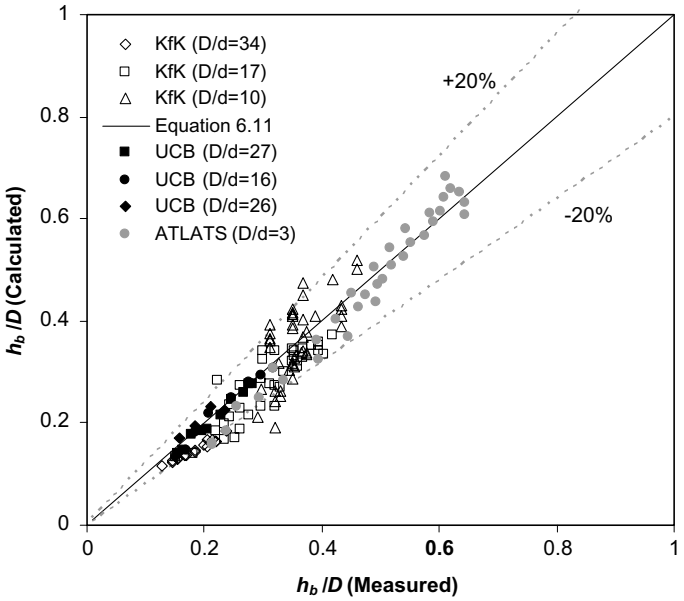

Fig. 7.3. Proposed entrainment onset criterion (Eq. (6.11)) vs. test data.

Fig. 7.1 shows the ability of the correlation of Smoglie and Schrock et al. to collapse the available data. Though the correlation works reasonably well for the data of Berkeley and KfK, it is not as good in predicting the ATLATS data, which were from a test tee section of larger branch size with respect to the size of the horizontal pipe ($D/d = 3$). Fig. 7.2 is a plot of the entrainment onset model developed by Maciaszek and Micaelli (1986) against the same test data employed in Fig. 7.1. The model predicts ATLATS data well, but cannot collapse the UCB and KfK data. It seems fair to conclude that the correlation of Schrock et al. and Smoglie is effective for small

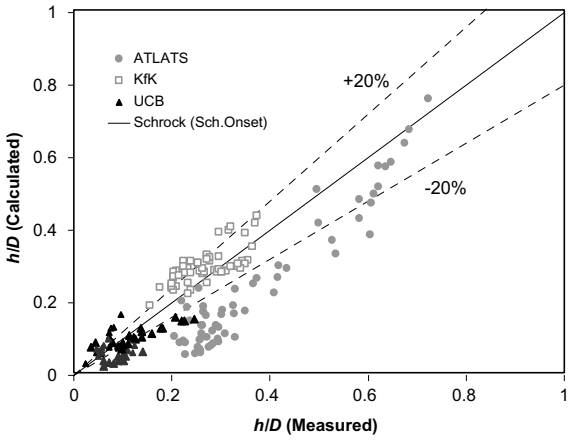

Fig. 7.4. Entrainment rate correlation of Schrock et al. vs. available test data.

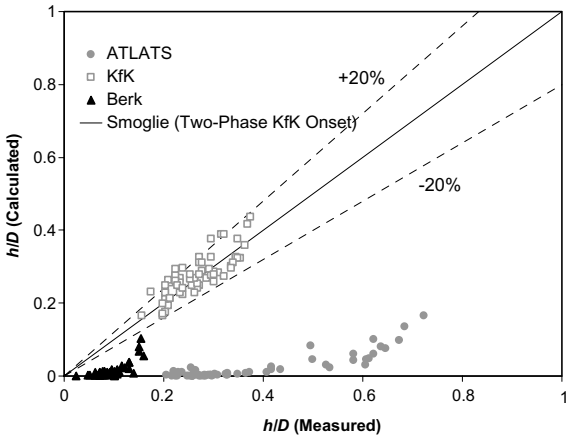

Fig. 7.5. Entrainment rate correlation of Smoglie vs. available test data.

branches ($D/d > 16$), whereas the correlation of Maziaszek et al. is applicable for large branches ($D/d < 7$).

The proposed liquid entrainment onset model is graphed in Fig. 7.3 along with the available data. Since the model has been derived for both small and large branch sizes, it collapses all the data within $\pm 20\%$. In other words, the new criterion asymptotically agrees with the previous correlations and unifies them through the derived combined potential and instability flow analysis. In addition, the proposed criterion accurately predicts the onset of entrainment in it's theoretically derived form and does not rely on any experimentally determined coefficients.

For the evaluation of different liquid entrainment rate correlations, the predicted and measured gas chamber heights are used in the comparisons (Figs. 7.4–7.7). The gas chamber height h was chosen for comparisons over the branch quality since it does not lump together the gas mass flow

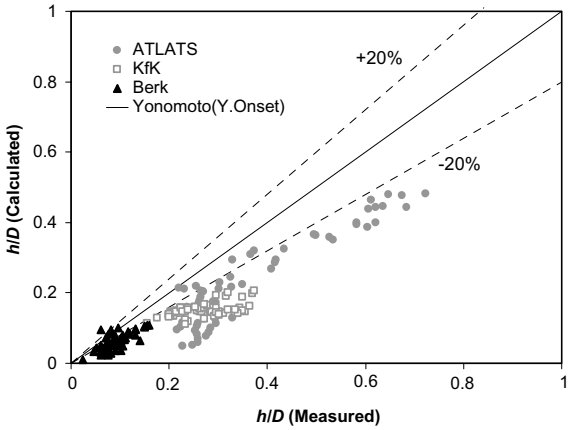

Fig. 7.6. Entrainment rate correlation of Yonomoto et al. vs. available test data.

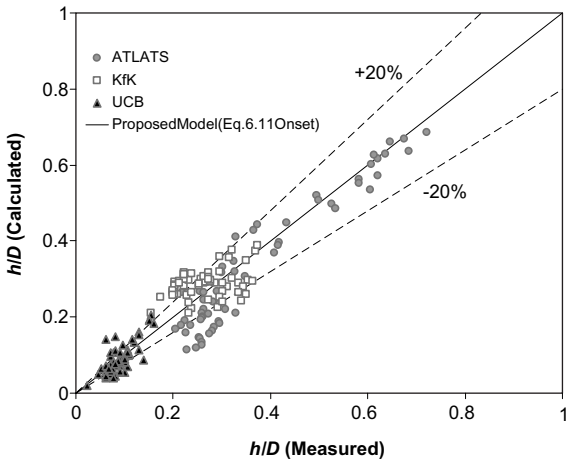

Fig. 7.7. Proposed entrainment rate correlation (Eq. (6.19)) vs. available test data.

rate w_{G3} and liquid mass flow rate w_{L3} which would make it difficult to distinguish between measured and calculated errors.

Fig. 7.4 is a graph of the correlation by Schrock et al. against the available test data. As expected, the correlation does a reasonable job in collapsing the UCB and KfK data, but has difficulty with the data from the ATLATS facility, which were obtained over a wider range of flow regimes. As the gas chamber height increases, the ATLATS data approaches the correlation. It perhaps is due to the distance of the interface level from the branch, thus the point sink approximation implied in the Schrock et al. correlation for h_b computation is marginally applicable. In Fig. 7.5, the correlation by Smoglie has difficulty in predicting all data except those produced at KfK. Yonomoto derived a model based on assuming a conical two-phase structure beneath the branch during steady-state liquid entrainment. The calculation of branch void fraction is similar to that chosen for the proposed model. Fig. 7.6 shows the ability of the model to collapse the data. However, a systematic shift is observed.

Finally, the proposed model is graphed in Fig. 7.7. The results indicate that the predictions of the new model agree marginally well with the available data. Scattering mainly occurs when the liquid-gas interface is close to the branch line inlet, due to the large fluctuation in liquid level. However, the new correlation collapses a wider range of data than previous correlations.

8. Concluding remarks

Experimental and theoretical investigations were conducted for the study of liquid entrainment in a tee junction with an upward-oriented vertical branch. The study included a comprehensive literature review, scaling analysis, experimental data, model improvement, and model evaluation.

It was found that the onset of entrainment measured in the scaled separate effects test facility (ATLATS) was more pronounced than in previous experiments due to the influence of branch size on the pressure drop across the tee test-section. During steady-state entrainment, a liquid slug formed in the hot leg and oscillated between the branch and steam generator inlet. This phenom-

enon, coupled with a larger branch size, resulted in liquid entrainment rates which on average were higher than in previous experimental studies. However, tests are being planned that will be run using the large integral test facility (APEX) at OSU. These tests will extend the current phase separation database to include effects of integral components and high temperature and pressure on liquid entrainment.

By combining the approaches of Smoglie and Maciaszek and Micaelli (1986), a new entrainment onset criterion was developed. The new criterion could be used for both small and large branch sizes. In fact, the correlations of Smoglie/Schrock et al. and of Maciaszek and Micaelli (1986) are representations of the two asymptotic solutions of the new correlation. Compared to the available experimental data for very different conditions, the new entrainment onset criterion collapsed those data within $\pm 20\%$. For the entrainment rate prediction, a new approach was proposed based on a potential flow simplification, and a comparison with the available test data showed a marked improvement. More importantly, the new model was able to collapse data of different test conditions, which could not be done with the existing correlations. It should be mentioned that scattering ($\sim 50\%$) still exists in the low gas flow quality range due to the large intermittency in the flow in the horizontal pipe. To reduce such a scattering, we believe that information regarding the degree of flow intermittency should be considered, which could require a second-order approach.

Acknowledgments

The authors are grateful to Jennifer Uhle, David Bessette, Joseph Kelly, Jack Rosenthal, and Farouk Eltawila of the US NRC for their technical guidance. Comments and encouragements from Graham Wallis, Virgil Schrock, Victor Ransom, Novak Zuber, and Sanjay Banerjee were deeply appreciated. We are also grateful to John Groome, Chris Gunderson, Teresa Culver, You Yao, and Hong Tang at Oregon State University for their outstanding support on this project.

References

Bharathan, D., Wallis, G.B., Richter, H.J., 1982. Lower plenum voiding. J. Heat Transfer 104, 479–486.

Ishii, M.K., 1993. Interficial area transport equation: preliminary considerations. Report of Nuclear Engineering Department, Purdue University, PU-NE-93/6, West Lafayette, ID 47907.

Kataoka, I., Ishii, M., 1987. Drift flux model for large diameter pipe and new correlation for pool void fraction. Int. J. Heat Mass Transfer 30, 1927–1939.

Maciaszek, T., Micaelli, J.C., 1986. The Cathre Phase Separation Model in Tee Junctions. SETh/LEML-EM/89-159.

Reimann, J., Khan, M., 1994. Flow through a small break at the bottom of a large pipe with stratified flow. Nuclear Science and Engineering 88, 297–310.

Rouse, H., 1956. Seven Exploratory Studies in Hydraulics. In: Proceedings ASCE, p. 82.

Schrock, V.E., Revankar, S.T., Mannheimer, R., 1986. Small break discharge—the roles of vapor and liquid entrainment in a stratified two-phase region upstream of the break. NUREG/CR-4761, LBL-22024.

Smoglie, C., 1984. Two-phase flow through small branches in a horizontal pipe with stratified flow. Dissertation, University of Karlsruhe.

Taitel, Y., Lee, N., Dukler, A.E., 1977. Gas-liquid transient flow in horizontal pipes: a model for predicting flow-pattern transitions. Final report. DOE/ID/01571-T1.

Todreas, Kazimi, 1988. Nuclear reactor thermal analysis. Hemisphere Publishing.

Yonomoto, T., Tasaka, K., 1988. New theoretical model for two-phase flow discharged from stratified two-phase region through small breaks. J. Nuclear Science Technology 25, 441–455.

Yonomoto, T., Tasaka, K., 1991. Liquid and gas entrainment to a small break hole from a stratified two-phase region. Int. J. Multiphase Flow 17, 745–765.

Wallis, G.B., 1969. One-dimensional two-phase flow. McGraw Hill.

Welter, K.B., 2002. Liquid entrainment at an upward oriented vertical branch line from a horizontal pipe. Ph.D. Dissertation, Oregon State University.

Wilson, G.E., Fletcher, C.D., Davis, C.B., Burtt, J.D., Boucher, T.J., 1997. Phenomena identification and ranking tables for Westinghouse AP600 small break loss-of-coolant accident, main steam line break, and steam generator tube rupture scenarios. NUREG/CR-6541, Review 2.

Zuber, N., 1980. Problems in modeling of small break LOCA. NUREG-0724.